J|A|C|S ARTICLES

Published on Web 04/29/2010

MASKE: Macroscopic Approach to Studying Kinetics at Equilibrium

Victor Okhonin, Maxim V. Berezovski,[§] and Sergey N. Krylov*

Department of Chemistry and Centre for Research on Biomolecular Interactions, York University, Toronto, Ontario M3J 1P3, Canada

Received January 6, 2010; E-mail: skrylov@yorku.ca

Abstract: The kinetics of biomolecular interactions at equilibrium is typically studied by "microscopic" methods that monitor concentration fluctuations of molecules in an "observation" volume in which the number of molecules is so small that the equilibrium is statistically impossible. Here, we introduce a "macroscopic" method for studying kinetics of biomolecular interactions at equilibrium which does not rely on monitoring the fluctuation of concentrations. We termed this method MASKE: a "macroscopic approach to studying kinetics at equilibrium". Conceptually, in MASKE, two equilibrium reaction mixtures, "unlabeled" and "labeled", are both prepared with two reactants and their complex; in the labeled mixture, one reactant is labeled for detection. A "macroscopic" amount of the labeled mixture is introduced into a long and narrow reactor filled with the unlabeled mixture, and a differential mobility of the reactant versus the complex is then induced by an external action along the reactor. The kinetics of complex formation and dissociation is then studied from the label-propagation pattern. In this work, we developed the theory of MASKE and experimentally proved it with a capillary as a reactor, a fluorophore as a label, and an electric field as a differential mobility inducer. Two pairs of molecules interacting with significantly different rate constants were used in this proof-of-principle work.

Introduction

The knowledge of rate and equilibrium constants of biomolecular interactions is pivotal to understanding the mechanisms of cellular processes and drug interactions with therapeutic targets.[1,2] The kinetics of such interactions is typically studied by monitoring changes in a reactant/product concentration after the reaction is perturbed from a chemical equilibrium.[3] For the sake of clarity, chemical equilibrium is defined as the state in which concentrations of reactants and products do not change with changing time and spatial coordinates. Perturbation from chemical equilibrium can cause changes in the structures of biopolymers (e.g., due to misfolding or aggregation) that can affect the kinetic parameters.[4−6] Such a perturbation creates concentration gradients and mass transfer against the gradients; the kinetics of mass transfer against the gradients may obscure the kinetics of the chemical reaction.[7] Finally, the "mathematics" of out-of-equilibrium reactions is inherently nonlinear, restricting the kinetic analysis to "nontransparent" numerical procedures.[8] As a result of the above limitations of nonequilibrium approaches, it is preferable to study the kinetics of biomolecular interactions in the state of chemical equilibrium.

The existing methods capable of studying kinetics at chemical equilibrium, for example fluorescence correlation spectroscopy (FCS),[9] nanopore amperometry,[10] and fluorescence resonance energy transfer (FRET),[11] are "microscopic" in their nature. They monitor concentration fluctuation in an observation volume in which the number of detected molecules is so small that equilibrium does not exist at any given time. The small number of molecules to be detected prevents the use of informative but less sensitive detection methods, such as mass spectrometry. Here, we introduce MASKE, the first "macroscopic approach to study kinetics at equilibrium", which monitors large numbers of molecules that can be detected with a wider scope of methods. At the conceptual level, in MASKE, two equilibrium reaction mixtures are prepared: "unlabeled" and "labeled". In the labeled mixture, one reactant is tagged with a detectable label that does not affect the complex formation and dissociation kinetics. As a result, both the reactant and the complex in the labeled mixture are labeled and detectable. The two mixtures are introduced, without mixing, into spatially distinct parts of a long and narrow reactor. Chemical equilibrium is maintained throughout the reactor as the two mixtures are kinetically identical; the label, on the other hand, occupies only a small part of the reactor

[§] Present address: Department of Chemistry, University of Ottawa, Ottawa, Ontario K1N 6N5, Canada.

(1) Chancellor, T. F., Jr.; Russell, R. J.; Dravid, V.; Lele, T. P. *Biotechnol. Prog.* **2008**, *24*, 89–95.
(2) Andersson, K.; Karlsson, R.; Loefaas, S.; Franklin, G.; Haemaelaeinen, M. D. *Exp. Opin. Drug Discovery* **2006**, *1*, 439–446.
(3) Bujalowski, W. *Chem. Rev.* **2006**, *106*, 556–606.
(4) Bates, G. P. *Science* **2006**, *311*, 1385–1386.
(5) Hammarstroem, P.; Wiseman, R. L.; Powers, E. T.; Kelly, J. W. *Science* **2003**, *299*, 713–716.
(6) Saluja, A.; Kalonia, D. S. *Int. J. Pharm.* **2008**, *358*, 1–15.
(7) Sigmundsson, K.; Masson, G.; Rice, R.; Beauchemin, N.; Oebrink, B. *Biochemistry* **2002**, *41*, 8263–8276.
(8) Avila, L. Z.; Chu, Y.-H.; Blossey, E. C.; Whitesides, G. M. *J. Med. Chem.* **1993**, *36*, 126–133.
(9) Al-Soufi, W.; Reija, B.; Novo, M.; Felekyan, S.; Kuhnemuth, R.; Seidel, C. A. M. *J. Am. Chem. Soc.* **2005**, *127*, 8775–8784.
(10) Hornblower, B.; Coombs, A.; Whitaker, R. D.; Kolomeisky, A.; Picone, S. J.; Meller, A.; Akeson, M. *Nat. Methods* **2007**, *4*, 315–317.
(11) Li, Y.; Augustine, G. J.; Weninger, K. *Biophys. J.* **2007**, *93*, 2178–2187.

10.1021/ja100104m

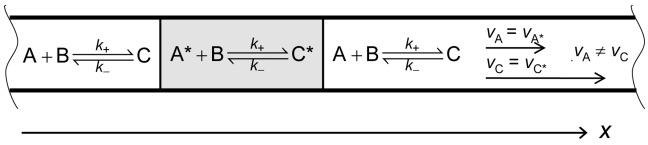

Figure 1. Schematic representation of MASKE setup in its initial condition. See text for details.

and, thus, is out of physical equilibrium. Finally, differential mobility of the reactant and product along the reactor is induced by an external action; the label must not affect the mobility of the reactant or complex. The combination of the dynamic equilibrium and differential mobility leads to a macroscopic change of the space shape occupied by the labeled reactant and labeled complex. The change is a function of the reaction rate constants, so the rate constants are directly determined from analysis of the label-propagation pattern along the reactor.

In this work, we first developed the theory of MASKE. The equilibrium nature of MASKE allowed us to find a general *analytical* solution for the label-propagation pattern. We used this solution to simulate and study spatial and temporal label-propagation patterns for different sets of conditions. We then developed two methods, one pattern-based and the other parameter-based, for finding the rate constants of complex formation and dissociation from the experimental label-propagation patterns. Finally, we experimentally proved the principle of MASKE by determining the kinetic parameters of noncovalent interactions in two pairs of molecules: (i) carbonic anhydrase II (CA) and its inhibitor, *N*-benzyl-4-sulfamoyl-benzamide, tagged with DNA (BSB-DNA), and (ii) β-cyclodextrin (β-CD) and cholesterol tagged with DNA (Chol-DNA). A long capillary was used as the reactor, a fluorescent dye was used as the label, and an electric field was used to induce differential mobility. The measurements were performed using a commercial capillary electrophoresis instrument without modification, suggesting that at least this mode of MASKE can be immediately practiced by researchers.

Results

Reactor, Reactants, and Reaction in MASKE: Theoretical Consideration. We consider the following theoretical setup (Figure 1). A single-dimensional infinite reactor is coaxial with the x coordinate. In such a reactor, in general, concentration gradients and mass transport are possible only along the x axis (a long capillary is a practical example of such a reactor). A binary reaction of reactant A reversibly binding reactant B and forming an affinity complex C, with rate constants of forward and reverse processes of k_+ and k_-, respectively, is in the state of chemical equilibrium:

$$\mathrm{A} + \mathrm{B} \underset{k_-}{\overset{k_+}{\rightleftharpoons}} \mathrm{C} \tag{1}$$

The equilibrium mixture of A, B, and C fills the entire reactor except for a finite part (gray area in Figure 1). This part is filled with a similar equilibrium mixture but with A, and accordingly C, being tagged with a detectable label (*) that does not affect k_+ and k_-:

$$\mathrm{A}^* + \mathrm{B} \underset{k_-}{\overset{k_+}{\rightleftharpoons}} \mathrm{C}^* \tag{2}$$

At time zero, A and C (and their labeled counterparts) start moving along x with nonequal velocities v_A and v_C, respectively. The label does not influence the velocities: $v_A = v_{A^*}$ and $v_C = v_{C^*}$.

Analytical Solution of Mass Transfer Equations in MASKE. The key point of our theoretical consideration is that the differential equations describing mass transfer of the labeled reactant and product (A* and C*) can be linearized. Their exact general solution (for concentrations of A* and C* as functions of time and a spatial coordinate) can be found *analytically* if the state of chemical equilibrium is maintained. The analytical solution could then facilitate comprehensive theoretical study of MASKE, which would be impossible if a numerical approach was used. The analytical solution could also facilitate simple approaches for finding k_+ and k_- from the experimental label-propagation patterns along the reactor.

The mass transfer of A* and C* is described by the following general system of differential equations:

$$\begin{aligned}(\partial_t + v_A\partial_x)A^* &= -k_+A^*B + k_-C^* \\ (\partial_t + v_C\partial_x)C^* &= k_+A^*B - k_-C^*\end{aligned} \tag{3}$$

where ∂_x and ∂_t are partial derivations by spatial coordinate and time, respectively, and A, A^*, B, C, and C^* are the concentrations of A, A*, B, C, and C*, respectively. In chemical equilibrium, the rates of the forward and reverse reactions are equal,

$$k_+(A^*(x) + A(x))B(x) = k_-(C^*(x) + C(x)) \tag{4}$$

and the concentrations of the reactants and product do not change with the space coordinate:

$$B(x) = \text{const}, \quad A^*(x) + A(x) = \text{const}, \quad C^*(x) + C(x) = \text{const} \tag{5}$$

Equations 3 are linear with respect to A^* and C^*, and exact analytical solutions for A^* and C^* can be found from them under conditions (5) (Supporting Information). Here, for simplicity, we designate these solutions as two linear functions of the initial conditions:

$$\begin{aligned}A^* &= A^*(x, t, B, v_A, v_C, k_+, k_-, \{A^*_0(x), C^*_0(x)\}) \\ C^* &= C^*(x, t, B, v_A, v_C, k_+, k_-, \{A^*_0(x), C^*_0(x)\})\end{aligned} \tag{6}$$

where $A^*_0(x)$ and $C^*_0(x)$ are time-independent initial x-distributions of reactants A* and C*. A sum of A^* and C^* found from **solution (6)** can be used to build simulated propagation patterns of the label in space and time domains. Next, we will analyze the simulated propagation patterns of A* and C* with the goal of finding generalities.

Theoretical Propagation Patterns of A* and C* in MASKE. We first consider spatial propagation patterns, which are "snapshots" of concentrations of A* and C* along the reactor; the spatial patterns are simpler for the conceptual analysis of MASKE than the temporal ones. At the qualitative level, the spatial propagation patterns of A* and C* can be understood even without analyzing **solution (6)**. There are two essential processes in the reactor: (i) dynamic equilibrium in reactions 1 and 2 and (ii) differential mobility of A* and C*. The propagation patterns of A* and C* depend on the relation between the characteristic equilibration time of the label between A* and C*, t_{eq}, and the characteristic separation time of A from C, t_{sep}. In MASKE, t_{eq} for label equilibration can be defined as (see the proof in the Supporting Information):

$$t_{eq} = 1/(k_+B + k_-) \tag{7}$$

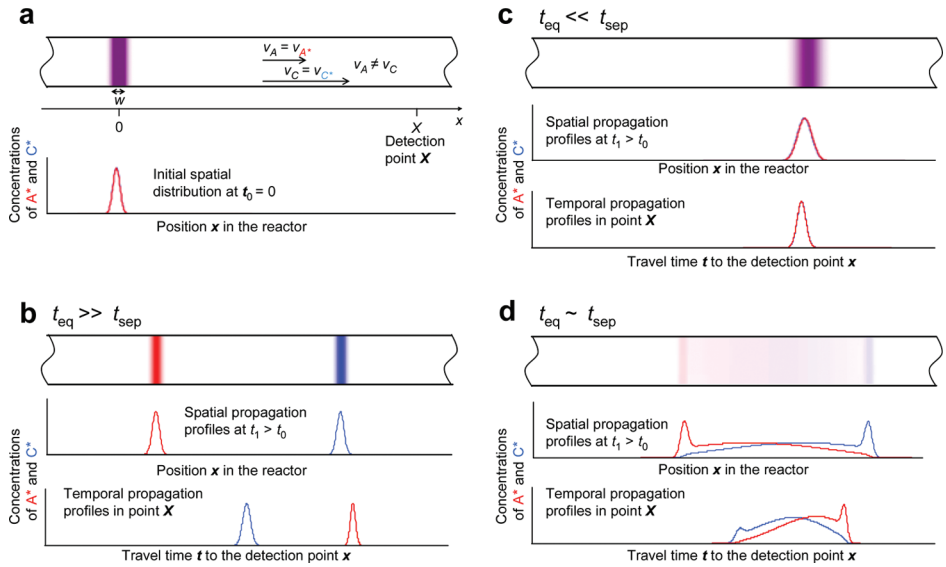

Figure 2. Illustration of spatial and temporal propagation patterns of A* and C* in a single-dimensional reactor for different relations between the characteristic equilibration time, t_{eq}, and the characteristic separation time, t_{sep}. (a) The initial spatial distribution of the labeled (A*, B, and C*) equilibrium mixture. (b−d) Three qualitatively different sets of spatial and temporal propagation patterns of A* and C* for three different relations between t_{eq} and t_{sep}: $t_{eq} \gg t_{sep}$, $t_{eq} \ll t_{sep}$, and $t_{eq} \sim t_{sep}$, respectively. The graphs in panels b−d were calculated with **solution (6)** using $t_{eq} = 200t_{sep}$, $0.02t_{sep}$, and $2t_{sep}$, respectively, travel time of C* to point X equal to $20t_{sep}$, $v_{C^*}/v_{A^*} = 1.5$, $B = K_d$, and the width of the initial Gaussian spatial distribution equal to 0.034 of the reactor's length (the width was defined for 1/e of the maximum concentration).

In general, equilibration time is defined as the time needed for the reaction to relax to equilibrium after a shift in any direction. In MASKE, the system is always at chemical equilibrium, and the only equilibration proceeding in it is the one of the label. In the other words, the systems in MASKE is out of "information" equilibrium and is proceeding to such equilibrium with the characteristic equilibration time shown in eq 7. The relationship between the relaxation to chemical equilibrium and the MASKE relaxation is further discussed in the Supporting Information (section 5).

The characteristic separation time, t_{sep}, is the time required for zones of A* and C* to separate from each other and can be defined as:

$$t_{sep} = w/(2|v_A - v_C|) \quad (8)$$

where w is the width of the initial zone of the labeled equilibrium mixture. If t_{eq} is much greater than t_{sep}, the zones of A* and C* will be separated before re-equilibration in reactions 1 and 2 proceeds to a significant extent. Thus, A* and C* will be moving as separate zones. If t_{eq} is much less than t_{sep}, the re-equilibration in reactions 1 and 2 occurs much faster than zone separation, and, as a result, A* and C* will be moving as a single zone. Finally, if t_{eq} does not differ much from t_{sep}, re-equilibration in reactions 1 and 2 and separation proceed with comparable rates. Therefore, A* and C* will be moving as two zones with some overlap between them. The depictions of a one-dimensional reactor in Figure 2 conceptually illustrate the propagation of zones of A* and C* for the three discussed relations between characteristic equilibration and separation times: $t_{eq} \ll t_{sep}$, $t_{eq} \gg t_{sep}$, and $t_{eq} \sim t_{sep}$.

At the quantitative level, the spatial propagation patterns of A* and C* can be constructed with **solution (6)** and presented as the dependencies of A^* and C^* on x for a fixed time t. We calculated $A^*(x)$ and $C^*(x)$ for a fixed time $t_1 > t_0$ and for the three different relations between the characteristic equilibration and separation times (Figure 2). The calculated x-dependencies of A^* and C^* confirmed the conclusions drawn from qualitative considerations. The two extreme cases of $t_{eq} \ll t_{sep}$ and $t_{eq} \gg t_{sep}$ correspond to the zones of A* and C* migrating separately and together, respectively. The intermediate case of $t_{eq} \sim t_{sep}$ corresponds to the partially overlapping zones.

While spatial propagation patterns are simpler for understanding the conceptual principles of MASKE, they are less important practically. Experimentally measuring spatial patterns requires obtaining a quantitative "image" of A* and C* distributions inside a reactor; this is impractical for the majority of detection approaches. For example, there is currently no practical way to take a spatial mass spectrometry image from inside a closed one-dimensional reactor. On the other hand, a temporal propagation pattern can be measured at a single point of the reactor (at the reactor's exit, for example, for the majority of available detection approaches: optical spectroscopy, mass spectrometry, radioactivity, and electrochemistry). Therefore, we will use temporal propagation patterns for the remainder of this work.

Temporal propagation patterns can be qualitatively presented as concentrations of A* and C* versus time required to travel distance X from the starting point to the detection point in the reactor. Figure 2 also shows temporal propagation patterns of A^* and C^* for the three ratios between t_{eq} and t_{sep} used for calculating the spatial patterns; these dependencies were also calculated using **solution (6)**.

Due to the linear relationship between the distance traveled and travel time, $x = vt$, the temporal patterns qualitatively resemble the spatial ones with a reversed order of zones. In the two extreme cases of $t_{eq} \ll t_{sep}$ and $t_{eq} \gg t_{sep}$, the zones of A* and C* migrate separately and together, respectively; in the intermediate case of $t_{eq} \sim t_{sep}$, the zones partially overlap. The patterns for nonextreme cases, when neither t_{eq} nor t_{sep} is much greater than the other one, can vary considerably depending on the difference between t_{eq} and t_{sep}, as shown in Figure S1 in the Supporting Information. Now that we understand how the propagation patterns of A* and C* can change with the changing ratio between t_{eq} and t_{sep}, we can develop methods for finding k_+ and k_- in MASKE.

All spatial and temporal propagation patterns in this work were calculated using **solution (6)** in an Excel spreadsheet provided in the Supporting Information (two versions, for Excel 2003 and Excel 2007; the same spreadsheet can also be found in the Research section of the authors' Web page: http://www.chem.yorku.ca/profs/krylov/).

Methods for Finding k_+ and k_- from the Label-Propagation Pattern in MASKE. A* and C* have the same label and can be experimentally undistinguishable. Therefore, our goal is to find the rate constants from experimental temporal propagation patterns of the label or, in other words, from experimental dependences of the label concentration on travel time, t, from the starting point to the detection point in the reactor. Finding k_+ and k_- from a label-propagation pattern is possible as the pattern explicitly depends on k_+ and k_- according to **solution (6)**.

We propose two general approaches to finding k_+ and k_- in MASKE: the pattern-based approach and the parameter-based approach. The pattern-based approach involves fitting the entire label-propagation pattern or part of it with a computer-simulated pattern while varying k_+ and k_- in the simulation. The values of the rate constants corresponding to the best fit are considered the correct ones. In the parameter-based approach, the rate constants are calculated using algebraic equations, utilizing two or more quantitative parameters obtained from the label-propagation patterns. Here, we present one pattern-based method and one parameter-based method.

The pattern-based method developed by us involves varying k_+ and k_- to achieve the minimum χ^2 for the deviation between the entire experimental label-propagation pattern and $A^*(t) + C^*(t)$ calculated from **solution (6)**. We designed software that can perform the curve-fitting task for varying k_+ and k_-. We then demonstrated the suitability of this pattern-based method and the correctness of the software. For this, label-propagation patterns for a wide range of t_{eq}/t_{sep} values were theoretically constructed (Figure S2a, Supporting Information). The values of k_+ and k_- were determined for these patterns using the pattern-based method. The method was shown to correctly determine k_+ and k_- for simulated temporal propagation patterns for t_{eq}/t_{sep} varying within 5 orders of magnitude (Figure S2b, Supporting Information). The best accuracy was obtained for $t_{eq} \sim t_{sep}$. The results of these numerical experiments suggest that both the algorithm and the software are correct.

The parameter-based method we developed allows K_d and k_- to be found for label-propagation patterns corresponding to fast re-equilibration, when t_{eq} is considerably shorter than t_{sep}. When such a condition is satisfied, the zones of A* and C* are not separated and appear as a single propagating zone of the label (Figure 2c). The pattern that contains a single zone is characterized by two parameters: the travel time, t, of the zone's center to the detection point at a distance X and the zone's temporal width, τ.

If these parameters can be determined experimentally and the prereaction concentrations of A and B, $A_0 = A + C$ and $B_0 = B + C$, are known along with the velocities of A and C, then K_d, k_-, and k_+ can be determined using the following equations (see eq 6.11 in the Supporting Information):

$$K_d = (X/t - v_C)\left(\frac{B_0}{v_A - X/t} - \frac{A_0}{v_A - v_C}\right)$$
$$k_- = \frac{4t(v_A - X/t)(v_C - X/t)^2}{(v_C - v_A)((X\tau_B/t)^2 - v_A^2\tau_{B=0}^2)}, \quad k_+ = k_-/K_d \tag{9}$$

where τ_B and $\tau_{B=0}$ are the widths of the label's zone in the presence and in the absence of B, respectively. To illustrate the suitability of this method, we used eq 9 to calculate K_d, k_-, and k_+ for the label-propagation patterns shown in Figure S2a in the Supporting Information. We found that the calculated constants deviated from constants used in the simulation by less than 10% if the label propagated as a single zone (Figure S2c, Supporting Information). The accuracy of this parameter-based method increases with decreasing t_{eq}/t_{sep}.

Other pattern- and parameter-based methods can be developed (such development is beyond the scope of this work). Due to their nature, pattern-based methods appear to be more generic than parameter-based methods. While pattern-based methods can be theoretically applied to all types of propagation patterns, parameter-based methods are applicable only to patterns that satisfy specific assumptions for which these methods are applicable. On the other hand, pattern-based methods require some expertise in numerical modeling, while parameter-based methods require no such expertise. In the next section, we use the two methods developed here in the experimental demonstration of MASKE.

When using the above methods for determining k_+ and k_- from experimental propagation patterns, one needs to appreciate that the accuracy of the resulting rate constants increases with increasing diversity of experimental data analyzed. One simple way to obtain diverse data in MASKE is to vary the concentration of B; such variation would generate different propagation patterns (see Figure S1 in the Supporting Information). The found values of k_+ and k_- are reliable only if the solution for k_+ and k_- (for patterns corresponding to different B) is stable. While varying B, we should ensure that k_+B does not dramatically differ from k_-. If k_+B significantly differs from k_-, then B also differs significantly from $K_d = k_-/k_+$. By using $A^* = C^*/(K_dB)$, we can conclude that, in such a case, A^* differs a great deal from C^*. In turn, if A^* is significantly different from C^*, then the smaller of them can be experimentally undetectable due to limited dynamic ranges of detectors. The approach of varying B was used in our experimental demonstration of MASKE below.

Experimental Models. In this proof-of-principle work, we chose an electric field to induce differential mobility of A* and C* and a fluorescent dye as a label. To work in a one-dimensional geometry, we conducted the study in a narrow (inner diameter of 75 μm) and long (50 cm) capillary reactor. Radial gradients of concentrations and radial mass transfer are negligible in such a capillary reactor. To exclude boundary effects in a finite-length capillary reactor, the ends of the capillary can be placed into reservoirs with the unlabeled equilibrium mixture. Advantageously, commercial capillary electrophoresis instruments with fluorescence detection can be used for such experiments. They are typically equipped with single-point detectors (located close to the end of the capillary) recording temporal label-propagation patterns. In this work, we used one such instrument without modifications.

Two experimental models, each involving a pair of molecules interacting with considerably different kinetics, were used: (i) carbonic anhydrase II (CA) and *N*-benzyl-4-sulfamoyl-benzamide tagged with 48-nt double-strand DNA (BSB-DNA) (Figure 3a), and (ii) β-cyclodextrin (β-CD) and cholesterol tagged with 23-nt single-stand DNA (Chol-DNA) (Figure 4a). The DNA tags had three important roles in our experiments. First, they were used as linkers for attaching a fluorescent label and spacing it from binding sites. This made the label's influence on the studied intermolecular interactions insignificant. Second, the relatively large and negatively charged DNA made the influence of the label on the electrophoresis

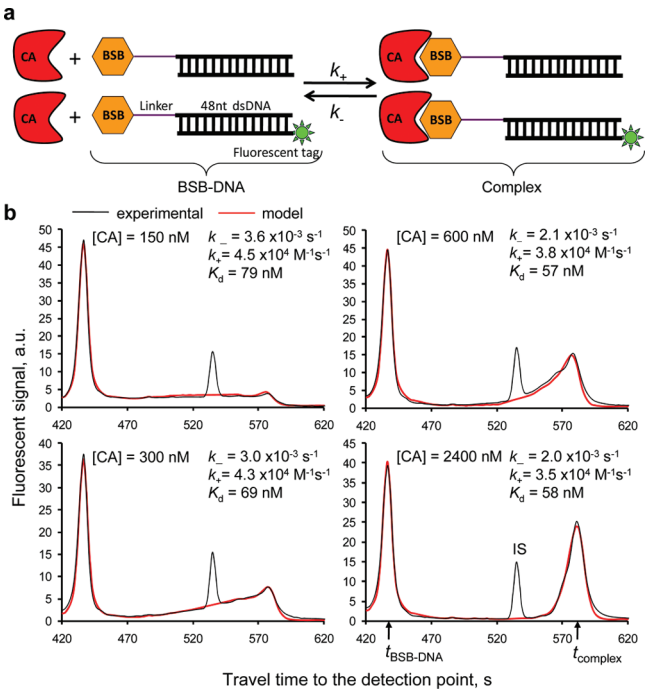

Figure 3. Determination of rate constants of complex formation and dissociation between CA and BSB-DNA by MASKE. (a) Schematic representation of the interacting molecules. (b) Representative temporal label-propagation patterns for varying concentration of CA. The black lines are the experimental data, while the red ones are the best fits obtained with the minimum χ^2 method. The rate constants correspond to the best fit.

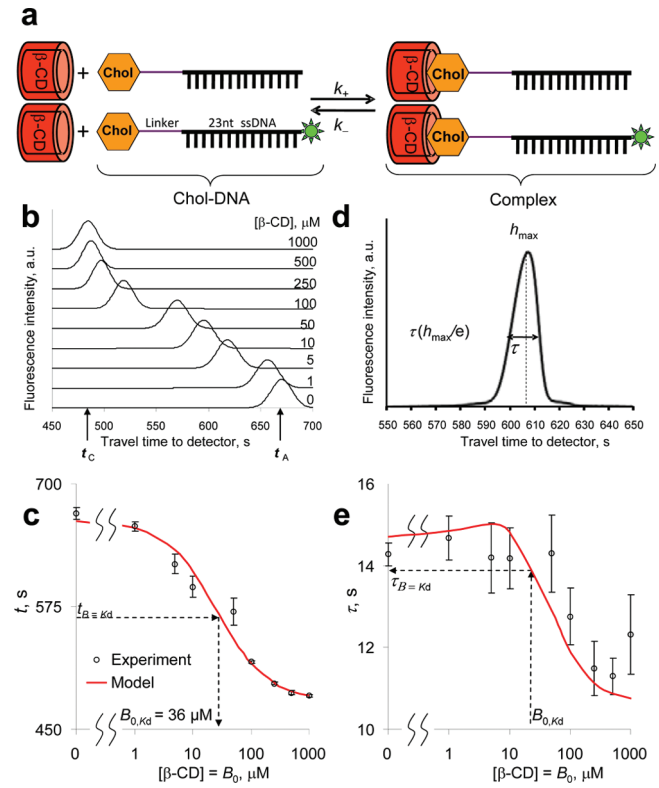

Figure 4. Determination of rate constants of complex formation and dissociation between β-CD and Chol-DNA by MASKE. (a) Schematic representation of the interacting molecules. (b) Representative temporal label-propagation patterns for varying concentration of β-CD. (c) The plot of travel time of the center of the label zone as a function of concentration of β-CD. The arrows illustrate a graphical approach of finding a B_0 value that corresponds to K_d. (d) Representative shape of the fluorescence signal from a label zone. The temporal width of the zone is found for the height equal to the maximum peak height, divided by the base of natural logarithm. (e) Dependence of the zone width on the concentration of β-CD. The arrows illustrate a method of finding the zone width that corresponds to $B = K_d$. This width is used to find k_-, and k_+ is calculated as k_-/K_d. The model lines in panels c and d were calculated with eqs 9, using the determined values of K_d and k_-.

mobility negligible. Finally, the highly polar DNA helped to dissolve cholesterol in an aqueous buffer. To stay consistent with the terminology used in the theoretical consideration, Chol-DNA and BSB-DNA are called A, while the labeled Chol-DNA and BSB-DNA are called A*. β-CD and CA are called B.

We confirmed that the label did not significantly influence the velocity of A by using light absorbance instead of fluorescence to facilitate the detection of both A and A*; our results confirmed that the assumption of $v_A = v_{A^*}$ was justified. Since C is heavier than A, the influence of the label on the velocity of C is even smaller; this justifies our assumption that $v_C = v_{C^*}$. In addition, by showing that the integrated fluorescence output of A* and C* did not depend of the concentration of B, we found that binding of B to A* did not quench fluorescence of A*. Otherwise, the difference in quantum yields would need to be included in **solution (6)**. Since the fluorescence label is separated from molecule A by a long DNA chain, we assumed that the label did not affect k_+ and k_-.

We have a few important notes on the choice of experimental conditions. The temperature for MASKE of the CA/BSB-DNA was chosen relatively low, 15 °C, to lower the k_- value and, thus, increase t_{eq}/t_{sep}. This was needed to demonstrate the experimental pattern with two well-resolved zones of A* and C*. The experimental conditions for the β-CD/Chol-DNA system were chosen to minimize the potential effect of three aggregation phenomena: (i) micelle formation by Chol-DNA, which could be considered as an ionic surfactant, (ii) duplex formation by two identical DNA strands which could have some matching bases in a sequence, and (iii) the formation of a complex of one Chol-DNA molecule with two molecules of β-CD.[12] First, the concentration of Chol-DNA was 100 nM, which is 4−5 orders of magnitude below typical critical micelle concentrations; this prevented micelle formation. Second, we excluded Na^+ from the run buffer to decrease the melting temperature of heteroduplexes of DNA from the calculated values of ~12 °C. This ensured that, at 20 °C, heteroduplex formation was negligible. Finally, we used a range of concentrations of β-CD (1 μM to 1 mM) well below concentrations of β-CD (>10 mM) at which the formation of 1:2 Chol-β-CD complex was observed.[12]

Experimental Label-Propagation Patterns and Determination of k_+ and k_-. Time profiles of label propagation for the two experimental models, CA/BSB-DNA and β-CD/Chol-DNA, were studied for varying concentrations of CA and β-CD (molecules designated as B) and are shown in Figures 3b and 4b, respectively. The patterns for the two models were found to be qualitatively different. The CA/BSB-DNA pattern clearly showed two separate zones of A* and C*. The increase in B increased the amount of C* formed but did not change the position of the zones. In contrast, the β-CD/Chol-DNA pattern had a single overlapping zone of A* and C*, and the position of this zone was shifting with increasing B. This behavior indicates that the CA/BSB-DNA model represents intermediate re-equilibration, while the β-CD/Chol-DNA model is an example of fast re-equilibration.

(12) Loftsson, T.; Magnusdottir, A.; Masson, M.; Sigurjonsdottir, J. F. *Pharm. Sci.* **2002**, *91*, 2307–2316.

Note that the orders of C and A in the patterns are different for the two experimental models: C migrated slower than A in the CA/BSB-DNA system and faster than A in the β-CD/Chol-DNA system. The explanation is in the differences in experimental conditions. CA/BSB-DNA was studied in a coated capillary without electroosmotic flow and with a negative electrode at the capillary inlet. β-CD/Chol-DNA was studied in an uncoated capillary with electroosmotic flow and with a positive electrode at the capillary inlet.

To determine k_+ and k_- for our first experimental model, we used the pattern-based method. Figure 3b compares experimental propagation patterns (black lines) and their best fits (red lines) obtained with **solution (6)** for the CA/BSB-DNA model; the peak of internal standard (IS) was excluded from the fitting. The results show high-quality fitting and reveal the rate constants; the equilibrium dissociation constants were calculated as k_-/k_+. Figure S3 in the Supporting Information shows similar data for two additional concentrations of CA. On the basis of the analysis of 21 experimental propagation patterns for a fixed concentration of A ($A_0 = 36$ nM) and seven different concentrations of B ($B_0 = 0$, 0.15, 0.3, 0.6, 1.2, 2.4, and 4.8 μM), we calculated average rate and equilibrium constants: $k_+ = (3.9 \pm 0.8) \times 10^4$ M^{-1} s^{-1}, $k_- = (2.6 \pm 0.6) \times 10^{-3}$ s^{-1}, and $K_d = 66.4 \pm 14.9$ nM. The values of k_+ and k_- have never been previously measured for this model. The results for K_d are in agreement with the previously reported ones for a higher temperature: the K_d for the higher temperature is higher.[13]

β-CD/Chol-DNA is a fast re-equilibration interacting pair for which our pattern-based method is applicable. Therefore, we used this method to find k_+ and k_- through a graphical approach (Figure 4b−e) explained in detail in the next two paragraphs.

First, we determine K_d using the following procedure. From Figure 4b, we find the migration times of A and C, t_A and t_C, for the zero and saturating concentrations of B, respectively. These migration times are used to determine the travel time of the zone's center when the concentration of B is equal to K_d:

$$t_{B=K_d} = 2t_A t_C/(t_A + t_C) \tag{10}$$

This formula is obtained from one of eqs 9 by assuming $B = K_d$; this condition leads to $X/t = (v_A + v_C)/2$, which is equivalent to eq 10. In addition, if $B = K_d$, then, at equilibrium, $A = C = A_0/2$, and, as a result, $K_d = B_0 - A_0/2$. We then use the data in Figure 4b to plot the travel time as a function of B_0 (Figure 4c) and determine the value of K_d in two steps, which take into account that $B \neq B_0$. Using arrows in Figure 4c, we find B_{0,K_d}, which correspond to $t_{B=K_d}$ determined in eq 10. Using the values of B_{0,K_d} and A_0, we calculate $K_d = B_{0,K_d} - A_0/2$.

Second, we find k_- with the following procedure. We define the zone's temporal width, τ, as corresponding to maximum fluorescence intensity, I_{max}, divided by the base of the natural logarithm (e $\approx$ 2.72) (Figure 4d). Since the zone's width increases with increasing residence time in the detection window, the changing residence time can be compensated for by multiplying it by t_A/t. Here t_A is the travel time of A without B, and t is the travel time of the label zone in the presence of B. Using the data in Figure 4b, we determine the experimental temporal widths and plot them as a function of B_0 ($B = B_0 - A/2$) (Figure 4e). With the arrows in Figure 4e, we find the zone's width corresponding to $B_0 = K_d + A_0/2$ (which is equivalent to $B = K_d$), $\tau_{B=K_d}$. Finally, $\tau_{B=K_d}$ is used to find k_-:

$$k_- = \frac{t^3_{B=K_d}(t_A - t_C)^2}{2t_C^2(\tau^2_{B=K_d}t_A^2 - \tau_A^2 t^2_{B=K_d})} \tag{11}$$

This formula is obtained from eq 9 by assuming $B = K_d$.

By using MASKE with the parameter-based method of constant determination, the rate and equilibrium constants were determined for the Chol-DNA/β-CD system: $k_- = 1.13 \pm 0.62$ s^{-1}, $K_d = 36.7 \pm 1.4$ μM, and $k_+ = (3.06 \pm 1.7) \times 10^4$ M^{-1} s^{-1}. To the best of our knowledge, this is the first report on the kinetic parameters for this molecular pair, which has prominent biological importance.[14] The constants were calculated on the basis of eight experiments repeated three times each with a fixed concentration of Chol-DNA ($A_0 = 100$ nM) and varying concentrations of β-CD ($B_0 = 0$, 1, 5, 10, 20, 100, 500, and 1000 μM).

It should be noted that molecular diffusion can contribute to zone widening in a similar way as molecular interaction. In our case, this contribution was negligible, as confirmed by no significant difference in rate constants determined with and without diffusion taken into account. Moreover, in our case, the zone became broader with decreasing propagation time—opposite to the phenomenon that could be caused by diffusion.

Discussion

We introduced the concept of MASKE, developed its theory, and demonstrated its practical application for long and narrow reactors. In MASKE, "long" means there are no boundary effects at the entrance and exit points of the reactor, and "narrow" means there are no radial concentration gradients and mass transfer. These conditions can be satisfied for different capillary dimensions depending on nongeometric parameters such as heat conductivity of the reactor walls and buffer and electrical conductivity of the buffer. Therefore, "long and narrow" cannot be strictly defined in terms of specific length and diameter of the reactor (or the length to diameter ratio). For practical consideration, capillaries typically used in capillary electrophoresis and capillary chromatography, length of 0.4−0.8 m and inner diameter of 20−75 μm, can be used as "long and narrow" reactors in all foreseeable experimental models.

While in our experimental demonstration of MASKE we used an electric field, other means of inducing differential mobility can theoretically be used, for example, separation by chromatography of centrifugation. It is difficult to speculate on advantages and limitations of different ways of separation *a priori*, but some general considerations can be made now. An external action used in MASKE to induce the differential mobility can potentially affect the reaction kinetics. While it has never been shown that an electric field can influence complex formation and/or dissociation, the possibility of such an influence cannot be completely excluded and must be experimentally studied. (Such studies are long overdue, considering the wide use of electrophoresis for studies of biomolecular interactions.) A similar concern exists for chromatography. The interaction of the reaction components with the chromatographic stationary phase can also affect the reaction kinetics. This effect will likely be small for mild modes of chromatography, such as size-exclusion. Centrifugation does not seem to have the above limitation but may have limited ability to separate complexes from free molecules.

While a fluorophore was used as a label in our proof-of-principle study, MASKE is theoretically compatible with other types of

(13) Drabovich, A. P.; Berezovski, M. V.; Musheev, M. U.; Krylov, S. N. *Anal. Chem.* **2009**, *81*, 490–494.

(14) Motoyama, K.; Kameyama, K.; Onodera, R.; Araki, N.; Hirayama, F.; Uekama, K.; Arima, H. *Eur. J. Pharm. Sci.* **2009**, *38*, 249–261.

labeling as well, for example, isotopic, electrochemical, and enzymatic. Accordingly, types of detection other than optical can be potentially used, including mass spectrometry. Isotopic labeling has the advantage of not influencing the reaction rate of differential mobilities of interacting molecules. Understanding other advantages and limitations of different ways of labeling and detection will require detailed comparative studies of them.

There is a family of nonequilibrium methods collectively termed kinetic capillary electrophoresis (KCE) that, similar to MASKE, utilize differential mobility to study reaction kinetics in a single-dimensional reactor.[15] In KCE, differential mobility is typically used to create conditions for the rate of either the forward or reverse process in reaction 1 becoming negligible. However, neither process can be disregarded for reactions with fast re-equilibration ($t_{eq} < t_{sep}$), thus making the perturbation methods inapplicable to such reactions. In contrast, being an equilibrium method, MASKE considers both the forward and reverse processes in reaction 1. It can, therefore, be applied to the widest range of reaction kinetics. Among these nonequilibrium methods, there is a quasi-equilibrium one in which a single reactant fills the reactor and the propagation of the second reactant through the first is followed while maintaining fast equilibrium.[16] The method is only applicable to fast equilibrium and is used for finding K_d only. However, Whitesides and coauthors, the pioneers of the approach, demonstrated its applicability to finding k_- and K_d through a relatively complicated numerical approach of analyzing reactant-propagation patterns.[8,17] The complexity of the analysis and the method's restriction to fast equilibration likely explain why the method has never been utilized thereafter. In general, nonequilibrium techniques are inherently nonlinear, making data analysis considerably more complex than in the "linear" MASKE.

To conclude, the availability of commercial instrumentation for capillary electrophoresis and high-performance liquid chromatography with all of the previously listed detection approaches suggests that multiple modes of MASKE can be exercised immediately. MASKE can potentially facilitate kinetic studies of macromolecular interactions in highly cooperative molecular "machines" for which classical perturbation methods are not applicable without changing machine components.

Materials and Methods

Chemicals and Materials. ssDNA-tagged cholesterol (Chol-DNA) with and without the 6-carboxyfluorescein (6-FAM) fluorophore at the 5′ end was purchased from IDT DNA Technologies (Coralville, IA): 5′-6-FAM-AGGGATTCCTGGGAAAACTGGAC-Chol and 5′-AGGGATTCCTGGGAAA ACTGGAC-Chol, respectively. Cholesterol was conjugated to the 3′ end of the 23-nt DNA sequence through a tetraethylene glycol linker. ssDNA-tagged *N*-benzyl-4-sulfamoyl-benzamide (BSB) was kindly provided by Ensemble Discovery (Cambridge, MA): 5′-BSB-CAGACGT-CACGCCAAACTCA CTACCAGCACTCTTCCGTCCACTACA-AC. BSB was conjugated to the 5′ end of the 48-nt DNA sequence through a polyethylene glycol linker.[18] A complementary 48-nt ssDNA sequence was purchased from IDT DNA Technologies, with and without the 6-FAM label at the 5′ end. Carbonic anhydrase II (CA) from bovine erythrocytes (M_r = 29 000 g/mol) and β-cyclodextrin β-CD (MW = 1135.01 g/mol) were from Sigma-Aldrich (Oakville, ON, Canada). The bare-silica capillary was purchased from Polymicro (Phoenix, AZ). Polyvinyl alcohol (PVA) and buffer components were obtained from Sigma-Aldrich. All solutions were made using deionized water filtered through a filter with a 0.22-μm pore size (Millipore, Nepean, ON, Canada).

Preparation of Unlabeled and Labeled Equilibrium Mixtures. The only difference between the unlabeled and labeled equilibrium mixtures was the fluorescent label on DNA-tagged cholesterol or DNA-tagged BSB. A 0.5 mL sample of the unlabeled and a 50 μL sample of the labeled equilibrium mixtures, containing 100 nM Chol-DNA and different concentrations of β-CD (0, 1, 5, 10, 20, 100, 250, 500, and 1000 μM), were prepared in the incubation/run buffer (50 mM Tris-acetate at pH 8.2) and incubated at 20 °C for 30 min to reach equilibrium. A 0.5 mL sample of the unlabeled and a 50 μL sample of the labeled equilibrium mixtures, containing 36 nM BSB-DNA and varying concentrations of CA (0, 150, 300, 600, 1200, 2400, and 5000 nM), were prepared in the incubation/run buffer and incubated at 15 °C for 30 min to reach equilibrium.

Experimental Conditions of MASKE. All MASKE experiments were performed with the following instrumentation, settings, and operations unless otherwise stated. MASKE was carried out with a P/ACE PA800 apparatus (Beckman Coulter, Mississauga, ON, Canada) equipped with absorption (260 and 490 nm) and fluorescence detectors (520 ± 10 nm); a 488-nm line of an Ar ion laser was utilized to excite fluorescence. For the β-CD/Chol-DNA experiments, we used the following conditions: an uncoated bare fused silica capillary maintained at 20 ± 0.5 °C, an electric field of 400 V/cm with a positive electrode at the injection end, the unlabeled equilibrium mixture in the inlet reservoir, and the incubation/run buffer in the outlet reservoir. For the CA/BSB-DNA experiments, we used the following conditions: a PVA-coated fused silica capillary with suppressed electroosmotic flow and temperature maintained at 15 ± 0.5 °C, an electric field of 400 V/cm with a positive electrode at the detection end, and the unlabeled equilibrium mixture in both the inlet and outlet reservoirs. PVA coating was carried out as described elsewhere.[19] For all experiments, the capillary was 50 cm long (40 cm to the detection window), with an inner diameter of 75 μm and an outer diameter of 360 μm. A 13-mm-long plug (26 nL) of the labeled equilibrium mixture was injected in the capillary from the inlet end by a pressure pulse of 5 s × 0.5 psi. Before each experiment, the capillary was rinsed with the incubation/run buffer for 5 min. The output data was fluorescence intensity at the detection point as a function of time passed since the application of the electric field.

Acknowledgment. This work was supported by grants from the Natural Sciences and Engineering Research Council of Canada.

Supporting Information Available: Analytical solution for kinetics in dynamic equilibrium, supporting figures, and spreadsheet (Excel 2003 and Excel 2007 versions) for calculation of propagation patterns. This material is available free of charge via the Internet at http://pubs.acs.org.

JA100104M

(15) Petrov, A.; Okhonin, V.; Berezovski, M.; Krylov, S. N. *J. Am. Chem. Soc.* **2005**, *127*, 17104–17110.
(16) *Affinity Capillary Electrophoresis in Pharmaceutics and Biopharmaceutics*; Drugs and the Pharmaceutical Sciences *128*; Neubert, R. H. H., Ruttinger, H.-H., Eds.; Marcel Dekker: New York, 2003.
(17) Chu, Y.-H.; Avila, L. Z.; Gao, J.; Whitesides, G. M. *Acc. Chem. Res.* **1995**, *28*, 461–468.
(18) Doyon, J. B.; Snyder, T. M.; Liu, D. R. *J. Am. Chem. Soc.* **2003**, *125*, 12372–12373.
(19) Gilges, M.; Kleemiss, M. H.; Schomburg, G. *Anal. Chem.* **1994**, *66*, 2038–2046.

SUPPORTING INFORMATION

Macroscopic Approach to Studying Kinetics at Equilibrium (MASKE)

Victor Okhonin[1], Maxim V Berezovski,[1,2] and Sergey N Krylov[1*]

[1]*Department of Chemistry and Centre for Research on Biomolecular Interactions, York University, Toronto, Ontario M3J 1P3, Canada*

[2]*Present address: Department of Chemistry, University of Ottawa, Ottawa, Ontario K1N 6N5, Canada*

Table of Contents

Supporting Analytical Solution for Kinetics in Dynamic Equilibrium

1. Equations of mass transfer for A* and C* and equilibrium conditions

We consider the theoretical setup presented in **Fig. 1** in main text. A single-dimensional infinite reactor is co-axial with the x coordinate. A binary reaction of A reversibly binding B and forming a complex C with rate constants of forward and reverse processes of k_+ and k_-, respectively, is in the state of chemical equilibrium:

$$\mathrm{A} + \mathrm{B} \underset{k_-}{\overset{k_+}{\rightleftharpoons}} \mathrm{C} \tag{1.1}$$

The equilibrium mixture of A, B, and C fills the entire reactor except for a finite part. This finite part is filled with a similar equilibrium mixture but with A, and accordingly C, being tagged with a detectable label (*), which does not affect k_+ and k_-:

$$\mathrm{A}^* + \mathrm{B} \underset{k_-}{\overset{k_+}{\rightleftharpoons}} \mathrm{C}^* \tag{1.2}$$

At time zero, A and C (and their labelled counterparts) start moving along the x axis with non-equal velocities v_A and v_C, respectively. The label does not influence the velocities so, $v_\mathrm{A} = v_{\mathrm{A}^*}$ and $v_\mathrm{C} = v_{\mathrm{C}^*}$. The mass transfer of A* and C* is described by the following system of differential equations:

$$\begin{aligned} (\partial_t + v_\mathrm{A}\partial_x)A^* &= -k_+ A^* B + k_- C^* \\ (\partial_t + v_\mathrm{C}\partial_x)C^* &= k_+ A^* B - k_- C^* \end{aligned} \tag{1.3}$$

where A, A^*, B, C, and C^* are concentrations of A, A*, B, C, and C*, respectively. In chemical equilibrium, the rates of the forward and reverse reactions are equal:

$$k_+(A^*(x) + A(x))B = k_-(C^*(x) + C(x)) \tag{1.4}$$

and the concentrations of the reactants and complex do not change with the coordinate:

$$\begin{aligned} B(x) &= const \\ A^*(x) + A(x) &= const \\ C^*(x) + C(x) &= const \end{aligned} \tag{1.5}$$

Our goal is to analytically solve Equations (1.3) for A^* and C^*, using the equilibrium conditions (1.4) and (1.5), and the above assumptions.

2. Dimensionless equations

We define new independent variables:

$$\begin{aligned} \varepsilon &= \sqrt{k_+ B / k_-}, & \lambda &= \sqrt{k_+ k_- B}, \\ \tau &= t\lambda, & y &= \left(2x - (v_\mathrm{A} + v_\mathrm{C})t\right)\lambda / (v_\mathrm{A} - v_\mathrm{C}) \end{aligned} \tag{2.1}$$

In these variables, equations (1.3) can be written as:

$$\begin{aligned} (\partial_\tau + \partial_y + \varepsilon)A^* &= C^* / \varepsilon \\ (\partial_\tau - \partial_y + 1/\varepsilon)C^* &= A^* \varepsilon \end{aligned} \tag{2.2}$$

For further simplification, we substitute variables A^* and C^* with new variables $\boldsymbol{a}$ and $\boldsymbol{c}$:

$$\begin{aligned} a &= A^* \exp\left((\varepsilon + 1/\varepsilon)\tau/2 + (\varepsilon - 1/\varepsilon)y/2\right) \\ c &= C^* \exp\left((\varepsilon + 1/\varepsilon)\tau/2 + (\varepsilon - 1/\varepsilon)y/2\right) \end{aligned} \tag{2.3}$$

Note that due to the linearity of equations (1.3) and (2.2), dimension of concentrations in them can be changed arbitrarily by dividing the equations by any constant value with a required dimension.

For the variables defined in (2.3), equations (2.2) can be written as:

$$(\partial_\tau + \partial_y)a = c/\varepsilon$$
$$(\partial_\tau - \partial_y)a = c\varepsilon \tag{2.4}$$

According to (2.4), we have standard Klein-Gordon equations for variables ***a*** and ***c*****:**

$$(\partial_\tau^2 - \partial_y^2)a = a$$
$$(\partial_\tau^2 - \partial_y^2)c = c \tag{2.5}$$

Dimensionless equations (2.4) and (2.5) will be solved in the next section.

3. Solution of dimensionless equations

We will find specific solutions of equations (2.5) for the case of an extremely sharp initial zone of A* and C* (A* and C* initially occupy the same zone). These specific solutions can be also used as Green's function, which allows us to find a general solution for given arbitrary initial conditions. Specifically, we will find solutions for two types of initial conditions:

$$a(0,y) = \delta(y), \quad c(0,y) = 0 \tag{3.1}$$

and

$$a(0,y) = 0, \quad c(0,y) = \delta(y) \tag{3.2}$$

Taking into account the relation between ***a*** and ***c*** described by equation (2.4), we can rewrite conditions (3.1):

$$a_1(0,y) = \delta(y), \quad (\partial_\tau + \partial_y)a_1(\tau,y)\big|_{\tau=0} = 0$$
$$c_1(\tau,y) = \varepsilon(\partial_\tau + \partial_y)a_1(\tau,y) \tag{3.3}$$

and conditions (3.2):

$$c_2(0,y) = \delta(y), \quad (\partial_\tau - \partial_y)c_2(\tau,y)\big|_{\tau=0} = 0$$
$$a_2(\tau,y) = (\partial_\tau - \partial_y)c_2(\tau,y)/\varepsilon \tag{3.4}$$

where indexes 1 and 2 correspond to the first (equation (3.1)) and second (equation (3.2)) types of initial conditions, respectively. Using Fourier decomposition of Dirac ***δ***–function for ***a*** and ***c*** from equations (3.3) and (3.4) we can get the solutions in a form of Fourier's integral:

$$a_1 = \frac{1}{4\pi}\int_{-\infty}^{\infty}\left\{(1-\frac{ik}{\sqrt{(1-k^2)}})\exp(\tau\sqrt{(1-k^2)}) + (1+\frac{ik}{\sqrt{(1-k^2)}})\exp(-\tau\sqrt{(1-k^2)})\right\}\exp(iky)dk \tag{3.5}$$
$$c_2 = \frac{1}{4\pi}\int_{-\infty}^{\infty}\left\{(1+\frac{ik}{\sqrt{(1-k^2)}})\exp(\tau\sqrt{(1-k^2)}) + (1-\frac{ik}{\sqrt{(1-k^2)}})\exp(-\tau\sqrt{(1-k^2)})\right\}\exp(iky)dk$$

where ***i*** is the imaginary unit and ***k*** is an internal parameter of integration. These expressions are equivalent to the following:

$$a_1 = (\partial_\tau - \partial_y)\frac{1}{2\pi}\int_{-\infty}^{\infty} \exp(iky)sh(\tau\sqrt{(1-k^2)})\frac{dk}{\sqrt{(1-k^2)}} \tag{3.6}$$
$$c_2 = (\partial_\tau + \partial_y)\frac{1}{2\pi}\int_{-\infty}^{\infty} \exp(iky)sh(\tau\sqrt{(1-k^2)})\frac{dk}{\sqrt{(1-k^2)}}$$

where *sh* is the hyperbolic sine function. Let's define a new function:

$$I = \frac{1}{2\pi}\int_{-\infty}^{\infty} \exp(iky)sh(\tau\sqrt{(1-k^2)})\frac{dk}{\sqrt{(1-k^2)}} \tag{3.7}$$

For solving (3.6), it is sufficient to calculate integral (3.7), which is a solution of Klein-Gordon equations:

$$(\partial_\tau^2 - \partial_y^2 - 1)I(\tau, y) = 0 \tag{3.8}$$

In the rest of our consideration we will assume that dimensionless time τ is positive.

3a. The case of abs(*y*) > τ

Let's assume that:

$$abs(y) > \tau \tag{3.9}$$

In this case, integral (3.7) will be equal to zero. In order to prove this, we will use the following substitutions:

$$y = \rho ch(\beta), \tau = \rho sh(\beta)$$
$$k = \begin{cases} sign(\varphi)ch(\varphi), & abs(k) > 1 \\ \sin(\varphi), & abs(k) < 1 \end{cases} \tag{3.10}$$

where *sign* is a function equal to 1 for all positive arguments, equal to 0 for zero argument, and equal to -1 for negative arguments; *ch* is the hyperbolic cosine function; *k, ρ, φ ,* and β are new variables. In variables (3.10) , expression (3.7) has the form of:

$$I = \frac{1}{\pi}\int_0^{\infty} \cos(\rho ch(\beta)k)sh(\rho sh(\beta)\sqrt{(1-k^2)})\frac{dk}{\sqrt{(1-k^2)}} =$$
$$= \frac{1}{\pi}\int_0^{\infty} \cos(\rho ch(\beta)ch(\varphi))\sin(\rho sh(\beta)sh(\varphi))d\varphi + \tag{3.11}$$
$$+\frac{i}{\pi}\int_0^{\pi/2} \cos(\rho\cos(-i\beta)sin(\varphi))\sin(\rho\sin(-i\beta)\cos(\varphi))d\varphi =$$
$$= \frac{1}{\pi}\int_0^{\infty} \{\sin(\rho ch(\varphi+\beta)) - \sin(\rho ch(\varphi-\beta))\}d\varphi +$$
$$+\frac{i}{\pi}\int_0^{\pi/2} \{\sin(\rho\sin(\varphi - i\beta)) - \sin(\rho\sin(\varphi + i\beta))\}d\varphi$$

Expression (3.11) can be transformed, by using an integral on a contour in the complex plane for the last integral in expression (3.11), into expression:

$$I = \frac{-1}{2\pi}\int_{-\beta}^{\beta} \sin(\rho ch(\varphi))d\varphi + \frac{i}{2\pi}\int_{-\beta}^{\beta} \left\{\sin(\rho\sin(i\varphi)) - \sin(\rho\sin(i\varphi+\pi/2))\right\} d\varphi = 0 \tag{3.12}$$

where the following equality was used:

$$\int_{0}^{\pi/2} \left\{\sin(\rho\sin(\varphi-i\beta)) - \sin(\rho\sin(\varphi+i\beta))\right\} d\varphi = \int_{-i\beta}^{\pi/2-i\beta} \sin(\rho\sin(\varphi))d\varphi + \int_{\pi/2+i\beta}^{i\beta} \sin(\rho\sin(\varphi))d\varphi = \tag{3.13}$$
$$= \int_{-i\beta}^{i\beta} i\sin(\rho\sin(\varphi))d\varphi - \int_{\pi/2-i\beta}^{\pi/2+i\beta} i\sin(\rho\sin(\varphi))d\varphi = \int_{-\beta}^{\beta} i\sin(\rho\sin(i\varphi))d\varphi - \int_{-\beta}^{\beta} i\sin(\rho\cos(i\varphi))d\varphi$$

3b. The case of abs(y) < τ

Now, let's assume that:

$$abs(y) < \tau \tag{3.14}$$

In this case, integral (3.7) will not be equal to zero. In order to calculate the integral, we can use the following substitution:

$$y = \rho sh(\beta), \quad \tau = \rho ch(\beta)$$
$$k = \begin{cases} sign(\varphi)ch(\varphi), & abs(k) > 1 \\ \sin(\varphi), & abs(k) < 1 \end{cases} \tag{3.15}$$

With variables (3.15), expression (3.7) has the form:

$$I = \frac{1}{\pi}\int_{0}^{\infty} \cos(\rho sh(\beta)k)sh(\rho ch(\beta)\sqrt{(1-k^2)})\frac{dk}{\sqrt{(1-k^2)}} =$$
$$= \frac{1}{\pi}\int_{0}^{\infty} \cos(\rho sh(\beta)ch(\varphi))\sin(\rho ch(\beta)sh(\varphi))d\varphi + \tag{3.16}$$
$$+ \frac{i}{\pi}\int_{0}^{\pi/2} \cos(i\rho\sin(-i\beta)sin(\varphi))\sin(-i\rho\cos(-i\beta)\cos(\varphi))d\varphi =$$
$$= \frac{1}{2\pi}\int_{0}^{\infty} \left\{\sin(\rho sh(\varphi+\beta)) + \sin(\rho sh(\varphi-\beta))\right\} d\varphi +$$
$$+ \frac{i}{2\pi}\int_{0}^{\pi/2} \left\{\sin(-i\rho\cos(\varphi-i\beta)) + \sin(-i\rho\cos(\varphi+i\beta))\right\} d\varphi$$

Expression (3.16) can be transformed, using an integral on a contour in a complex plane for the last integral in expression (3.16), into expression:

$$I = \frac{1}{\pi}\left(\int_0^{\infty} \sin(\rho sh(\varphi))d\varphi + \int_0^{\pi/2} sh(\rho\cos(\varphi))d\varphi \right) \tag{3.17}$$

where we used the following equality:

$$\begin{aligned}
&\int_0^{\pi/2} \left\{ \sin(-i\rho\cos(\varphi - i\beta)) + \sin(-i\rho\cos(\varphi + i\beta)) \right\} d\varphi = \\
&= 2\int_0^{\pi/2} \sin(-i\rho\cos(\varphi))d\varphi - \int_0^{i\beta} \sin(-i\rho\cos(\varphi))d\varphi - \\
&- \int_0^{-i\beta} \sin(-i\rho\cos(\varphi))d\varphi - \int_0^{i\beta} \sin(-i\rho\sin(\varphi))d\varphi - \\
&- \int_0^{-i\beta} \sin(-i\rho\sin(\varphi))d\varphi = \\
&= -2i\int_0^{\pi/2} sh(\rho\cos(\varphi))d\varphi - 2i\int_0^{\beta} \sin(\rho sh(\varphi))d\varphi
\end{aligned} \tag{3.18}$$

According to the expression (3.17), ***I*** does not depend on τ and ***y*** separately, but rather depends on ρ only. Using (3.8), we can obtain the following equation for $I(\rho)$:

$$I''(\rho) + I'(\rho)/\rho - I(\rho) = 0 \tag{3.19}$$

with the boundary condition:

$$I(0) = \frac{1}{\pi}\int_0^{\infty} \sin(x)\frac{dx}{x} = \frac{1}{2} \tag{3.20}$$

Equation (3.19) with boundary condition (3.20) indicates that ***I*** is proportional to the Macdonald's function of the zero order I_0:

$$I(\rho) = I_0(\rho)/2 \tag{3.21}$$

Also, for derivative of ***I*** by ρ, we have:

$$I'(\rho) = I_1(\rho)/2 \tag{3.22}$$

where function I_1 is the Macdonald's function of the first order.

As a result, for the arbitrary values of τ and ***y***, we have expression:

$$I(\tau,y)=I_0(\sqrt{\tau^2-y^2})\theta(\tau-y)\theta(\tau+y)/2$$
$$(\partial_\tau+\partial_y)I(\tau,y)=\sqrt{\frac{\tau-y}{\tau+y}}I_1(\sqrt{\tau^2-y^2})\theta(\tau-y)\theta(\tau+y)/2+I_0(0)\delta(\tau+y)\theta(\tau-y) \quad (3.23)$$
$$(\partial_\tau-\partial_y)I(\tau,y)=\sqrt{\frac{\tau+y}{\tau-y}}I_1(\sqrt{\tau^2-y^2})\theta(\tau-y)\theta(\tau+y)/2+I_0(0)\delta(\tau-y)\theta(\tau+y)$$

where

$$\theta(x)=\begin{cases}0, x<0\\ 1, x>0\end{cases} \quad (3.24)$$

4. Transformation of dimensionless solution into a solution with original variables

According to equations (3.3) and (3.4), equation (3.23) will have two types of solutions:

$$\begin{cases}a_1=I_1(\rho)\sqrt{\left(\frac{\tau+y}{\tau-y}\right)}/2+\delta(\tau-y)\\ c_1=\varepsilon I_0(\rho)/2\end{cases} \quad (4.1)$$

and

$$\begin{cases}a_2=I_0(\rho)/(2\varepsilon)\\ c_2=I_1(\rho)\sqrt{\left(\frac{\tau-y}{\tau+y}\right)}/2+\delta(\tau+y)\end{cases}$$

where solution $\boldsymbol{a_1}$, $\boldsymbol{c_1}$ corresponds to the initial concentration of $\boldsymbol{c}$ equal to zero, and solution $\boldsymbol{a_2}$, $\boldsymbol{c_2}$ corresponds to the initial concentration of $\boldsymbol{a}$ equal to zero.

According to equation (2.3), and by using equation (2.1), for $\boldsymbol{A}^*$ and $\boldsymbol{C}^*$we can write:

$$A_1^*=\left(\frac{|\omega|}{2}\sqrt{\frac{\eta}{\mu}}I_1(\rho)+\delta(\mu)\right)\gamma,\quad C_1^*=\frac{|\omega|\varepsilon}{2}I_0(\rho)\gamma$$
$$A_2^*=\frac{|\omega|}{2\varepsilon}I_0(\rho)\gamma,\quad C_2^*=\left(\frac{|\omega|}{2}\sqrt{\frac{\mu}{\eta}}I_1(\rho)+\delta(\eta)\right)\gamma \quad (4.2)$$

where

$$\varepsilon=\sqrt{k_+B/k_-},\quad \omega=2\sqrt{k_+k_-B}/(v_A-v_C)$$
$$\mu=v_At-x,\quad \eta=x-v_Ct,\quad \rho=|\omega|\sqrt{\mu\eta}$$
$$\varphi=\omega(\varepsilon-1/\varepsilon)/2,\quad \psi=\omega(v_C\varepsilon-v_A/\varepsilon)/2,\quad \gamma=\exp(t\psi-x\varphi)$$

Here, solution $\boldsymbol{A}^*_1$, $\boldsymbol{C}^*_1$ corresponds to the initial condition:

$$A_1^*(x,0) = \delta(x), \quad C_1^*(x,0) = 0 \tag{4.3}$$

and solution $\boldsymbol{A}^*_2$, $\boldsymbol{C}^*_2$ corresponds to the initial condition:

$$A_2^*(x,0) = 0, \quad C_2^*(x,0) = \delta(x) \tag{4.4}$$

Conditions (4.3) and (4.4) correspond to two different types of Green functions. It should be noted that these conditions do not need to exist in reality as the above procedure of finding a solution of equations is purely mathematical. Solution (4.2) is the analytical solution sought in equation (1.3); this solution is presented in the main text as linear functionals of the initial conditions:

$$\begin{aligned} &A^*\left(x,t,B,v_A,v_C,k_+,k_-,\{A^*_0(x),C^*_0(x)\}\right) \\ &C^*\left(x,t,B,v_A,v_C,k_+,k_-,\{A^*_0(x),C^*_0(x)\}\right) \end{aligned} \tag{4.5}$$

where $A^*_0(x)$ and $C^*_0(x)$ are time-independent initial x-distributions of reactants A* and C*.

A sum of A^* and C^* found from equations (4.5) can be used to build simulated propagation patterns of the label in space- and time domains. For presentation in the space domain, we introduce a vector (grid) of space coordinates $\boldsymbol{x}_1 \ldots \boldsymbol{x}_n$ and use equation (4.5) to calculate the corresponding vectors of simulated concentrations. As a result, we obtain simulated distributions of concentrations of the labeled reactant, $A^*(x)$, and labeled product, $C^*(x)$, in the reactor, for any given time. A sum of $A^*(x)$ and $C^*(x)$ is termed the spatial label-propagation pattern. Alternatively, we can introduce a vector of times $\boldsymbol{t}_1 \ldots \boldsymbol{t}_n$, and calculate corresponding vectors of $A^*(t)$ and $C^*(t)$ for a fixed coordinate by using equation (4.5). A sum of $A^*(t)$ and $C^*(t)$ is a simulated temporal label-propagation pattern. Both types of patterns can be used to fit experimental data for finding the rate constants. For the benefit of the reader, we provide software which can be used to simulate spatial and temporal profiles of A^* and C^*.

5. Equilibrium (relaxation) time

5a. Relaxation process in a homogeneous case

In a homogeneous case, for a binary reaction, we will have a system of ordinary nonlinear differential equations:

$$d_t A = -k_+ AB + k_- C = d_t B = -d_t C \tag{5.1}$$

According to these equations, the sums A + C and B + C do not depend on time. Based on this, we can write a single equation:

$$d_t C(t) = k_+ (C(0) + A(0) - C(t))(C(0) + B(0) - C(t)) - k_- C \tag{5.2}$$

Equation for the equilibrium concentration of the complex, C', and expressions for the equilibrium concentrations of the reactants, A' and B', are:

$$\begin{aligned} &k_+ (C(0) + A(0) - C')(C(0) + B(0) - C') - k_- C' = 0 \\ &A' = C(0) + A(0) - C' \\ &B' = C(0) + B(0) - C' \end{aligned} \tag{5.3}$$

For an infinitesimal deviation of the complex concentration, δC, from chemical equilibrium, we can get from (5.2) and (5.3) the following equation:

$$d_t \delta C(t) = -\left(k_+ A' + k_+ B' + k_-\right)\delta C \equiv -\delta C / t_{eq}^h \tag{5.4}$$

According to this equation, the relaxation time to chemical equilibrium for a homogeneous case will be:

$$t_{eq}^h = 1/\left(k_+ B + k_+ A + k_-\right) \tag{5.5}$$

5b. Relaxation time for MASKE

Based on the following MASKE equations:

$$\begin{aligned}(\partial_t + v_{\mathrm{A}}\partial_x)A^* &= -k_+ A^* B + k_- C^* \\ (\partial_t + v_{\mathrm{C}}\partial_x)C^* &= k_+ A^* B - k_- C^*\end{aligned} \tag{5.6}$$

we can get equations for total amounts of C* and A*, defined as:

$$\begin{aligned}\mathrm{C}^*(t) &= \int C(x,t)dx \\ \mathrm{A}^*(t) &= \int A(x,t)dx\end{aligned} \tag{5.7}$$

where the interval of integration contains all regions of the reactor with non-zero concentration of the labeled reactant and complex. We additionally assume that at the boundaries of the integration interval, the concentrations of the labeled reactant and complex are equal to zero. In this case, for total amounts of A* and C* will be described by the ordinary linear differential equations:

$$\begin{aligned}d_t \mathrm{A}^* &= -k_+ \mathrm{A}^* B + k_- \mathrm{C}^* \\ d_t \mathrm{C}^* &= k_+ \mathrm{A}^* B - k_- \mathrm{C}^* = -d_t \mathrm{A}^*\end{aligned} \tag{5.8}$$

According to these equations, the sum of C* and A* doesn't depends on time. It allows us to get a single equation describing the process of relaxation:

$$d_t \mathrm{A}^*(t) = -\left(k_+ B + k_-\right)\mathrm{A}^*(t) + k_-\left(\mathrm{C}^*(0) + \mathrm{A}^*(0)\right) \tag{5.9}$$

Introducing the time of relaxation as:

$$t_{eq} = 1/\left(k_+ B + k_-\right) \tag{5.10}$$

we can present the relaxation equation in the following form:

$$d_t \mathrm{A}^*(t) = -\mathrm{A}^*(t)/t_{eq} + k_-\left(\mathrm{C}^*(0) + \mathrm{A}^*(0)\right) \tag{5.11}$$

By comparing equations (5.5) and (5.10) we can see that the relaxation times required for reaching chemical equilibrium and information equilibrium (MASKE) differ. This difference cab be easily interpreted: in MASKE, one of the reactants, B, is always in information (and chemical) equilibrium. As a result, reactant A does not influence the relaxation time to information equilibrium. Other differences are the following. In

MASKE, the simple relaxation equation exists only for total amounts for A* and C*, not for their concentrations. In the case of deviation from chemical equilibrium, the single equation exists for the concentrations. Also, in MASKE, there is no chemical non-equilibrium, so that there is no relaxation to chemical equilibrium. Instead, we have only "information" non-equilibrium, with relaxation of A* and C* but without any relaxation of A* + A and/or C* + C as they are constant.

6. Approximate solutions for the case of fast equilibration ($t_{eq} << t_{sep}$)

Let's introducing new variables:

$$s = A^* + C^*, \quad j = v_A A^* + v_C C^* \tag{6.1}$$

By using these variables, equations (1.3) can be presented in the form of:

$$\begin{aligned} &\partial_t s + \partial_x j = 0 \\ &\partial_t j + \partial_x (j(v_C + v_A) - suv_A) + j(Bk_+ + k_-) - s(Bk_+ v_C + k_- v_A) = 0 \end{aligned} \tag{6.2}$$

For the case of large $Bk_+ + k_-$ (corresponding to small equilibration time, $t_{eq} << t_{sep}$, where $t_{eq} = 1/(Bk_+ + k_-)$), we can use an approximate equation for j:

$$j \approx s\frac{Bk_+ v_C + k_- v_A}{Bk_+ + k_-} - \frac{Bk_+ k_- (v_C - v_A)^2}{(Bk_+ + k_-)^3}\partial_x s \tag{6.3}$$

By substituting equation (6.3) into equation (6.2), we can obtain another approximate equation:

$$\partial_t s = -\partial_x s\frac{Bk_+ v_C + k_- v_A}{Bk_+ + k_-} + \frac{Bk_+ k_- (v_C - v_A)^2}{(Bk_+ + k_-)^3}\partial_x^2 s \tag{6.4}$$

The last equation describes the transfer of a sum density of A* and C* with average velocity:

$$V = (Bk_+ v_C + k_- v_A)/(Bk_+ + k_-) \tag{6.5}$$

and a dispersion coefficient (which has the same units as the diffusion coefficient and can be used in the equation of diffusion) for zone widening:

$$\mu = Bk_+ k_- (v_C - v_A)^2/(Bk_+ + k_-)^3 \tag{6.6}$$

Equation (6.5) is equivalent to:

$$V = (v_C B/K_d + v_A)/(B/K_d + 1) \tag{6.7}$$

Equation (6.6) can, in turn, be transformed to:

$$\mu = \frac{B/K_d}{(B/K_d + 1)^3}\frac{(v_C - v_A)^2}{k_-} \tag{6.8}$$

In the described case, the zones of A* and C* propagate as single zone. The average velocity of this zone is described by expression (6.7); and zone broadening depends on the virtual diffusion coefficient described by equation (6.8).

7. Determination of K_d and k_- for the case of fast equilibration

If the zones of A* and C* move with the average velocity described by equation (6.7), they will reach a detection point at a distance X from the beginning of the reactor in time T defined as X/V:

$$T = X\left(B + K_\mathrm{d}\right)/\left(v_\mathrm{C}B + v_\mathrm{A}K_\mathrm{d}\right) \tag{7.1}$$

If T is experimentally determined, then K_d can be found from equation (7.1).

Now, if K_d is known, equation (6.8) can be used to determine k_-. For experimental determination of the dispersion coefficient μ, we can use the dependence of zone broadening (caused by this dispersion) on time:

$$w_t^{\,2} = w_0^2 + 4t\mu \tag{7.2}$$

where $\boldsymbol{w_t}$ is the spatial width of the zone as a function of time $\boldsymbol{t}$ and $\boldsymbol{w_0}$ is the initial zone width at the inlet of the reactor. The spatial width is defined as the zone's width at which the label concentration equals to 1/e of the maximum one. Using equation (7.2), we can express k_- through zone broadening:

$$k_- = \frac{B/K_\mathrm{d}}{(B/K_\mathrm{d}+1)^3}\frac{4t(v_\mathrm{C}-v_\mathrm{A})^2}{\left(w_t^{\,2}-w_0^2\right)} \tag{7.3}$$

Concentration of free $\boldsymbol{B}$ can be expressed through total concentrations of B and A, $\boldsymbol{B}_0$ and $\boldsymbol{A}_0$, respectively:

$$\begin{aligned} &K_\mathrm{d}C = AB, \quad (V-v_\mathrm{C})B = (v_\mathrm{A}-V)K_\mathrm{d} \Rightarrow (V-v_\mathrm{C})C = (v_\mathrm{A}-V)A, \\ &A = A_0 - C \Rightarrow C = \frac{v_\mathrm{A}-V}{v_\mathrm{A}-v_\mathrm{C}}A_0 \Rightarrow B = B_0 - C = B_0 - A_0\frac{v_\mathrm{A}-V}{v_\mathrm{A}-v_\mathrm{C}}, \end{aligned} \tag{7.4}$$

Using the following equality:

$$\frac{B}{K_\mathrm{d}} = \frac{v_\mathrm{A}-V}{V-v_\mathrm{C}} \tag{7.5}$$

K_d can then be expressed as a function of B_0:

$$K_\mathrm{d} = (V-v_\mathrm{C})\left(\frac{B_0}{v_\mathrm{A}-V} - \frac{A_0}{v_\mathrm{A}-v_\mathrm{C}}\right) \tag{7.6}$$

For sharp zone boundaries, the temporal width, $\boldsymbol{\tau}$, of the zone relates to the spatial zone width, $\boldsymbol{w}$, as:

$$\tau = w/V \tag{7.7}$$

where $\boldsymbol{V}$ is the average velocity of the zone propagation. If the concentration of B is equal to zero, there should be no broadening of the label zone due to the reaction between A and B, and the spatial width of the zone at the detection point should, thus, be equal to the initial width of the zone at the reactor's inlet. We do not take into account broadening due to diffusion since it is negligible under the experimental conditions of

this work. As a result, for the initial width of the zone (if injection conditions, determining the initial width for the zone, do not depend on *B*), using equation (7.7), we can get the following expression:

$$w_0 = \tau_{B=0} v_A \tag{7.8}$$

Using equations (7.7) and (7.8), expression (7.3) can be rewritten as:

$$k_- = \frac{B / K_d}{(B / K_d + 1)^3} \frac{4t(v_C - v_A)^2}{\left((\tau_B V)^2 - (\tau_{B=0} v_A)^2\right)} \tag{7.9}$$

For the sharp zones, the velocity can be found by expression:

$$v = X / t \tag{7.10}$$

where ***X*** is distance from initial position of zone's "summit" (maximum label concentration) to the detection point, and ***t*** is time required for the zone's summit to reach the detection point. By using equation (7.10), expressions (7.6) and (7.9) can be rewritten as:

$$\begin{aligned} K_d &= (X / t - v_C)\left(\frac{B_0}{v_A - X / t} - \frac{A_0}{v_A - v_C}\right) \\ k_- &= \frac{4t(v_A - X / t)(v_C - X / t)^2}{(v_C - v_A)\left((X\tau_B / t)^2 - v_A^2 \tau_{B=0}^2\right)} \\ k_+ &= k_- / K_d \end{aligned} \tag{7.11}$$

These equation (which appear as equations (9) in main text) are used in the parameter-based method, which utilizes the temporal propagation patterns obtained in the case of fast equilibration.

Supporting Figures

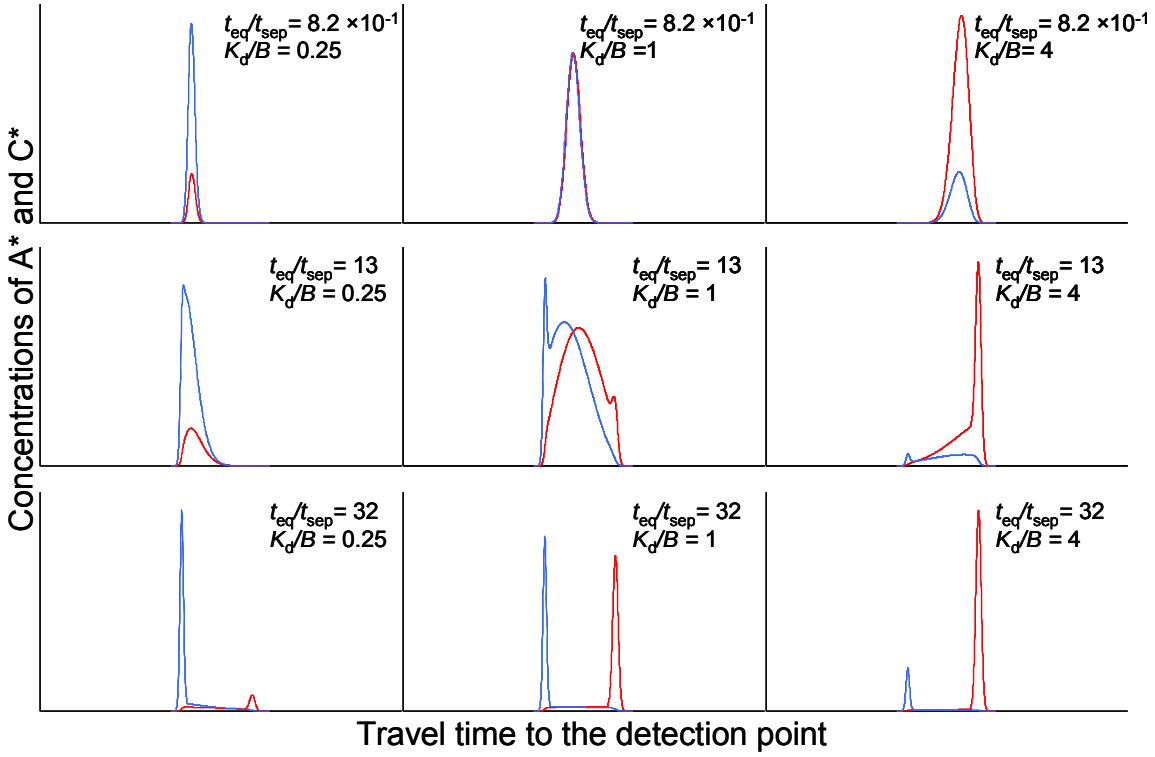

Figure S1. Simulated dimensionless temporal propagation patterns of A* (red) and C* (blue) in a single-dimensional reactor for varying ratios between: (i) the characteristic equilibration time (t_{eq}) and the characteristic separation time (t_{sep}) and (ii) the equilibrium dissociation constant (K_d) and concentration of B (B). $A^*(t)$ and $C^*(t)$ were calculated by using equations (4.2). In all cases, the travel time of C* to reach the detection point was 20 × t_{sep}, v_{C^*}/v_{A^*} was 1.5, and the initial concentration distributions for A* and C* were identical and had the Gaussian shape with a width of 0.034 of the reactor length (the width was defined for 1/e = 0.367879… of the maximum concentration).

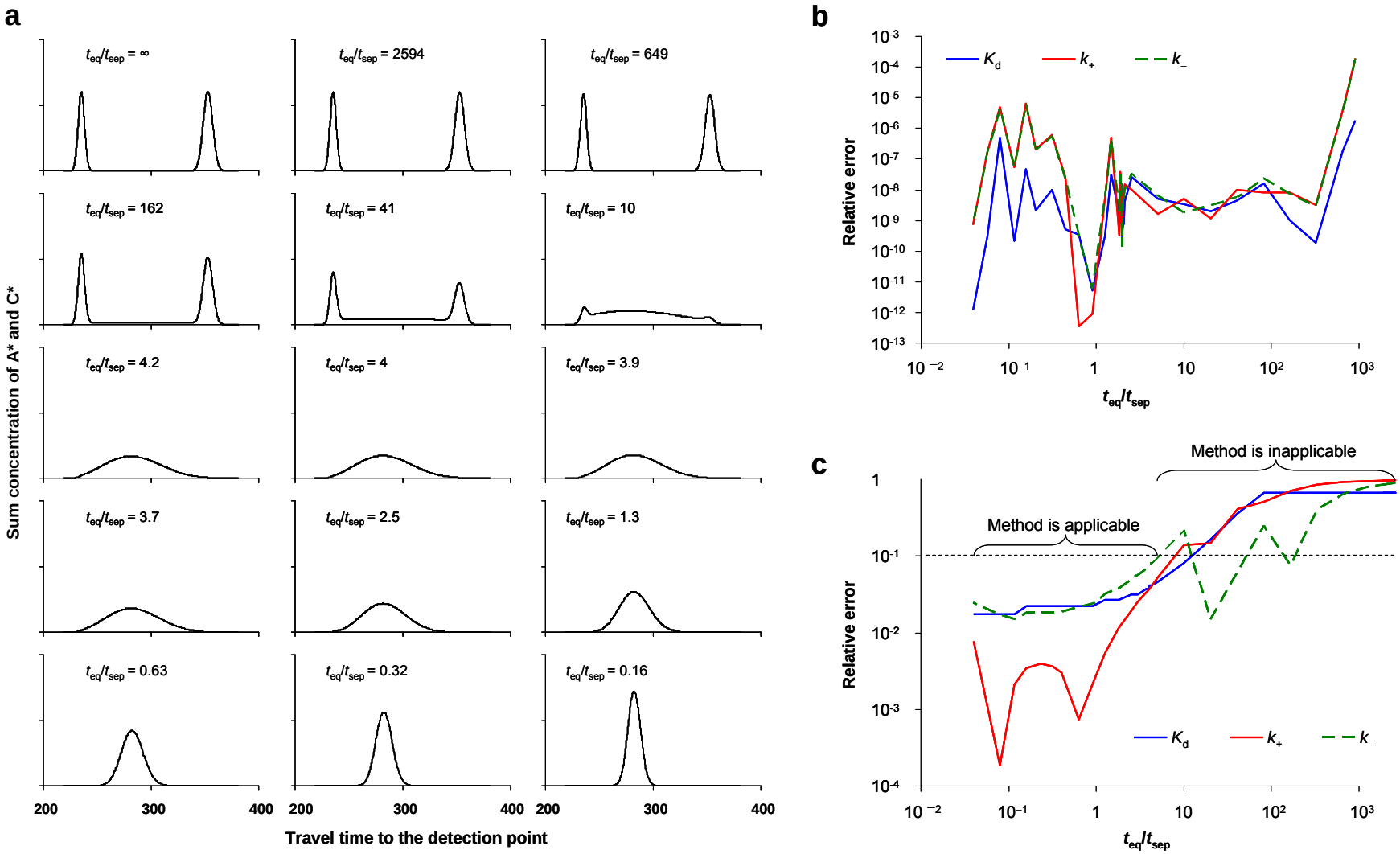

Figure S2. Evaluation of methods for finding constants K_d, k_-, and k_+ by using the simulated label-propagation patterns. **(a)** Temporal label-propagation patterns, $A^*(t) + C^*(t)$, simulated with equation (4.2) for different values of t_{eq}/t_{sep} and for $B = K_d$. The conditions of simulation were identical to conditions used in Supplementary Fig. 1. **(b)** Inaccuracy of the pattern-based method. The found constants were those corresponding to final fits of the patterns shown in panel (a) using the minimum χ^2 criterion. The fitting was performed by Excel Solver with Solver's precision setup at a level of 10^{-13} and starting values of K_d and k_- being two times smaller than the exact K_d and k_- used for simulating patterns in panel (a). **(c)** Inaccuracy of the parameter-based method assuming unresolved zones of A* and C* which appear as a single peak. The values of k_- and K_d were determined using equations (6.11). In both panels (b) and (c), the values of k_+ were calculated as k_-/K_d and the relative errors were found as absolute values of the following ratio: (found constant – exact constant)/(found constant + exact constant).

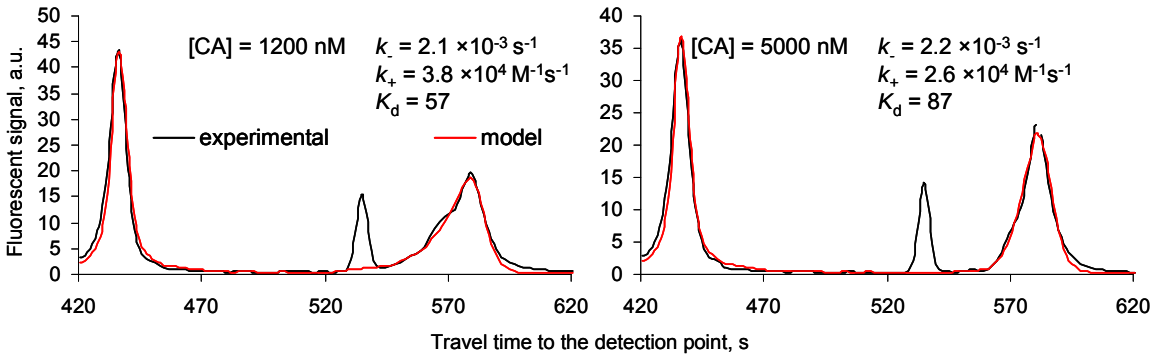

Figure S3. Determination of rate constants of complex formation and dissociation between CA and BSB-DNA by MASKE for CA concentrations of 1.2 and 5.0 μM. The black lines are the experimental data while the red once are the best fits obtained with the minimum χ^2 method. The rate constants correspond to the best fit.